Bioorganic & Medicinal Chemistry 17 (2009) 7884–7893

Contents lists available at ScienceDirect

Bioorganic & Medicinal Chemistry

journal homepage: www.elsevier.com/locate/bmc

N-Acylpolyamine inhibitors of HDM2 and HDMX binding to p53

Ryo Hayashi [a], Deyun Wang [b], Toshiaki Hara [a], Jaclyn A. Iera [b], Stewart R. Durell [a], Daniel H. Appella [b,*]

[a] Laboratory of Cell Biology, NCI, NIH, DHHS, Bethesda, MD 20892, United States
[b] Laboratory of Bioorganic Chemistry, NIDDK, NIH, DHHS, Bethesda, MD 20892, United States

ARTICLE INFO

Article history:
Received 14 August 2009
Revised 14 October 2009
Accepted 15 October 2009
Available online 21 October 2009

Keywords:
HDMX
HDM2
Cancer
Protein–protein interactions

ABSTRACT

Selective inhibition of protein–protein interactions important for cellular processes could lead to the development of new therapies against disease. In the area of cancer, overexpression of the proteins human double minute 2 (HDM2) and its homolog HDMX has been linked to tumor aggressiveness. Both HDM2 and HDMX bind to p53 and prevent cell cycle arrest or apoptosis in damaged cells. Developing a strategy to simultaneously prevent the binding of both HDM2 and HDMX to p53 is an essential feature of inhibitors to restore p53 activity in a number of different cancers. Inhibition of protein–protein interactions with synthetic molecules is an emerging area of research that requires new inhibitors tailored to mimic the types of interfaces between proteins. Our strategy to create inhibitors of protein–protein interactions is to develop a non-natural scaffold that may be used as a starting point to identify important molecular components necessary for inhibition. In this study, we report an *N*-acylpolyamine (NAPA) scaffold that supports numerous sidechains in a compact atomic arrangement. NAPAs were constructed by a series of reductive aminations between amino acid derivatives followed by acylation at the resulting secondary amine. An optimized NAPA was able to equally inhibit the association of both HDM2 and HDMX with p53. Our results demonstrate some of the challenges associated with targeting multiple protein–protein interactions involved in overlapping cellular processes.

Published by Elsevier Ltd.

1. Introduction

The protein p53 acts as a cellular guardian against proliferation of damaged cells.[1] In healthy cells, p53 is inactivated by several negative regulators, allowing cells to proliferate.[2] Under conditions of cellular stress or genomic damage, p53 is activated and functions to promote cell cycle arrest or apoptosis. In the majority of cancers, p53 activity is defective due either to a genetic mutation in p53 that prevents DNA binding or to the overexpression of negative regulators of p53 (such as HDM2 and HDMX).[3] Overexpression of HDM2 and HDMX has been linked to tumor aggressiveness and drug resistance, and inhibition can restore p53 function and prevent cancer growth.[2,4,5] HDM2 acts as a ubiquitin ligase upon binding to p53, targeting p53 for degradation.[2] Recently, several studies have highlighted the importance of HDMX as a negative regulator of p53.[4,6,7] HDMX binds to p53 at the same site as HDM2, but it lacks ubiquitin ligase activity and therefore blocks p53 activity without promoting degradation.[8] Although the regulation of HDM2 and HDMX is complex, blocking association of both proteins with p53 seems to be essential in order to restore p53 activity in a number of cancers.[9]

The complex formed between HDM2 and p53 has served as a paradigm for chemists to develop molecules that are tailored to inhibit protein–protein interactions. A crystal structure of the complex formed between HDM2 (residues 17–125 of the N-terminal domain) and a peptide derived from the transactivation domain of p53 (residues 15–29)[10] highlighted the following important features of this protein–protein interaction: HDM2 has a large hydrophobic cleft that binds to p53, p53 adopts an amphipathic α-helix between residues 18–26, and p53 projects three hydrophobic residues from the α-helix (F19, W23 and L26) so that they pack tightly and deeply in the non-polar cleft of HDM2. The stability of the p53–HDM2 complex is primarily due to the hydrophobic interactions involving the three cleft-binding residues, as confirmed by amino acid substitution studies.[11] This structure greatly stimulated the search for HDM2 inhibitors with chemotherapeutic activity, and much success has been achieved in this area.[12,13] The best inhibitors of HDM2–p53 binding are either small molecules that are very hydrophobic or oligomeric molecules that arrange hydrophobic sidechains into the same three-dimensional arrangement as the bound p53 helix. One of the best small molecule inhibitors of HDM2–p53 binding is Nutlin-3.[14] This molecule, along with a few other inhibitors of HDM2, have demonstrated efficacy in multiple cell-based systems and a few animal models of cancer tumors.[15–18] However, Nutlin-3 and the other HDM2 inhibitors only weakly inhibit HDMX binding to p53, and this deficiency could ultimately prevent development of Nutlin-3 and other HDM2 inhibitors into effective chemotherapeutic drugs.[6,19]

A comparison of the structures of HDM2 and HDMX indicates the reason that Nutlin-3 shows diminished inhibition of HDMX–

* Corresponding author.
E-mail address: appellad@niddk.nih.gov (D.H. Appella).

0968-0896/$ - see front matter Published by Elsevier Ltd.
doi:10.1016/j.bmc.2009.10.032

p53 association.[20,21] Within the p53-binding sites of the two proteins, HDMX has a significantly smaller hydrophobic binding cleft due primarily to the protrusion of the sidechain of tyrosine 96 into this area. The corresponding sidechain in HDM2 (tyrosine 100) is rotated away from the binding cleft.[20] Nevertheless, the structure of the complex between the p53 peptide and HDMX is very similar to the p53–HDM2 complex. In both structures, the same series of hydrophobic sidechains from the p53 α-helix protrude into the binding clefts and there are only slight perturbations in the helical structure to accommodate the differences between the two binding sites, consistent with the similar affinities of the p53 peptide for HDM2 and HDMX.[22] Based on the structure, it has been proposed that the protrusion of tyrosine 96 into the binding cleft sterically clashes with Nutlin-3 to weaken the binding to HDMX.[21]

Therefore, the development of inhibitors of both HDM2 and HDMX binding to p53 is becoming an important new target for chemists to tackle.[23] Recently, the work of Schepartz and co-workers has elegantly demonstrated that helical β-peptides can be appropriately modified to bind with good affinity to both HDM2 and HDMX.[24] Here, we report an alternative scaffold based on the β-sheet tri-urea template developed by Nowick et al.[25] Among the inhibitors of p53–HDM2, Robinson showed that peptide-based structures other than a helix can be developed into inhibitors.[26] In this work, cyclic peptides in β-sheet conformations were developed into very potent inhibitors of HDM2–p53 association.[27–29] Based on these precedents, we have developed a scaffold we have termed *N*-acylpolyamines (NAPAs, Fig. 1) and we have optimized the sidechains projecting from the scaffold to inhibit both HDM2 and HDMX binding to a p53 peptide with IC_{50} values around 2 μM. As illustrated in Figure 1, our general strategy was to project hydrophobic sidechains from the urea (R_i) to bind into the proteins' hydrophobic binding clefts while sidechains attached to the carbon backbone (R_o) would be hydrophilic and exposed to the solvent. Our results indicate that it is possible to develop non-peptidic synthetic molecules with equal inhibitory activity against both HDM2 and HDMX binding to p53.

2. Experimental

2.1. Molecular modeling

Models of the complexes of the different NAPA derivatives and HDM2 and HDMX were developed to be analogous to a number of crystal structures of these proteins with peptides and Nutlin. These included the following entries in the RCSB Protein Data Bank:[30] 1YCR,[10] 1RV1,[14] 2Z5T,[21] 3DAB and 3DAC,[20] 3EQS and 3EQY[31] and 3G03 and 3FD0.[32] The coordinates of the NAPA compounds were developed with the 2D and 3D editor modules of the Quanta 2006 software package (Accelrys, Inc., San Diego, CA). The models were energy minimized with the CHARMM molecular mechanics computer program and the CHARMM22 versions of the all-atom topology and parameter sets.[33] The complexes were than further optimized using the AUTODOCK 4 software package with the Lamarckian GA algorithm (Scripps Research Institute, La Jolla, Ca).[34] Illustrations of the models were created with the Chimera software program (University of California, San Francisco, CA).[35] Modeling was used to examine the conformational-range of possible complexes consistent with the experimental results of the different NAPA analogs and to help design better binding analogs. No attempt was made to predict the 'best' complex structure from calculation of the binding energies.

2.2. Solid phase NAPA synthesis

See Supplementary data for details on general methods and preparation of amino aldehydes. TentaGel R resin, Rink type (25 μmol, substitution 0.17–0.20 mmol/g) was allowed to swell in NMP in a 10 mL disposable filter polypropylene column (Pierce Biotechnology Inc., Rockford, IL) for 1 h. β-Alanine was coupled to the resin by the HBTU–HOBt method. The coupling protocol was as follows: (i) deprotection of the Fmoc group with 20% piperidine in NMP for 10 min; (ii) washing with NMP (×5); (iii) activation of *N*-α-Fmoc-protected amino acid (0.25 mmol) with 0.45 M HBTU–HOBt solution in DMF (0.56 mL, 0.25 mmol), and 2 M DIEA solution in NMP (0.5 mmol, 500 μL) for 10 min; (iv) coupling with the pre-activated *N*-α-Fmoc-protected amino acid for 40 min; and (v) washing with NMP (×5). The synthetic protocol for urea derivatives was as follows: (i) deprotection of the Fmoc group in the above condition; (ii) washing with NMP (×5) and then with dry DCM (×5); (iii) addition of *N*-α-Fmoc-protected amino aldehyde (0.25–0.35 mmol) to the resin as a 0.25–0.5 M solution in dry DCM, followed by acetic acid (7 μL, 0.125 mmol); (iv) after shaking for 1 h, all solvent was drained, and the resin was rinsed with dry DCM (×5); (v) addition of $NaBH(OAc)_3$ (53 mg, 0.25 mmol) to the resin as a 0.25 M solution in DCM; (vi) shaking for 2 h, and then washing with NMP (×5) and with dry DCM (×5); (vii) addition of 0.5 M isocyanate solution in dry DCM (0.25–0.50 mmol) and *N*-methylmorphorine (28 μL, 0.25 mmol); and (viii) shaking for 2 h, and then washing with DCM (×5) and NMP (×5). The above steps were repeated three times. After removing the Fmoc group, 2,4-dimethoxybenzylisocyanate (21 μL, 0.25 mmol was added to the resin as a 0.5 M solution in dry DCM, followed by *N*-methylmorphorine (28 mL, 0.25 mmol). To add a urea bond or a peptide bond at the R_4 position, isocyanate or carboxylic acid were reacted under the above conditions. The mixture was shaken for 1–2 h. Final deprotection and cleavage of the urea derivatives from the resin were achieved with 94% TFA/5% water/1% TIS for 2 h at room temperature. After removing the resin by filtration, the filtrate was

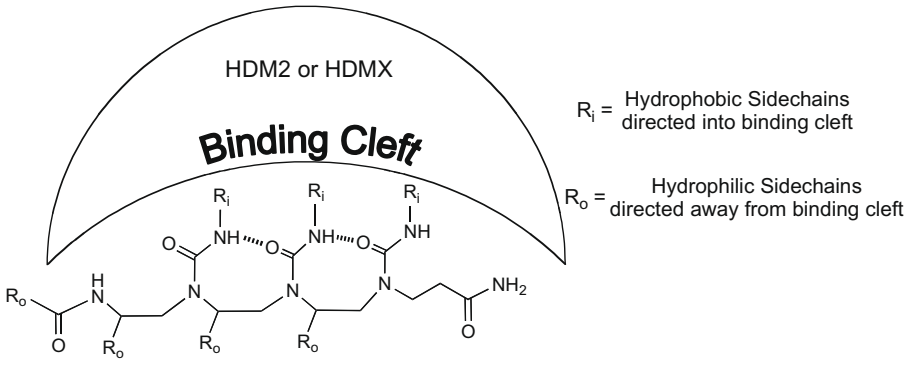

Figure 1. Schematic representation of idealized NAPA binding to HDM2 or HDMX with intramolecular hydrogen bonds between the urea sidechains that direct the hydrophobic sidechains into the binding cleft of the proteins. The hydrophilic sidechains are designed to be solvent exposed.

concentrated with nitrogen gas, and the crude product was precipitated by diethyl ether. Obtained crude products were purified by preparative HPLC on a Vydac Protein C4 column (22 × 250 mm i.d.) using the following solvent systems: (A) water containing 0.05% TFA; (B) acetonitrile containing 0.04% TFA. The purity of the oligourea was confirmed by analytical HPLC on a Vydac Protein C4 column (4.6 × 250 mm i.d.) and an Agilent XDB-C18 column (4.6 × 250 mm i.d.) using the same solvent systems as described above. HPLC-purified urea derivatives were characterized by ESI or MALDI-TOF mass spectroscopy.

2.3. Protein expression

The HDM2(11–119) and HDMX(1–188) were expressed in *Escherichia coli* BL21 (DE3) as a GST fusion protein in pGEX4T-1 (GE Healthcare, Arlington, VA) and purified on glutathione sepharose. The HDM2(11–119) was cleaved from the GST on the resin using thrombin. The GST-HDMX(1–188) was eluted with reduced glutathione-containing phosphate buffered saline. The obtained proteins were >90% pure as assessed by SDS–PAGE analysis. The concentration was determined by A_{280} and the Bradford protein assay.

2.4. Binding assays

Inhibitory activities of NAPAs were measured by fluorescence anisotropy competition experiments as previously described.[36] After NAPAs were dissolved in water or DMSO as approximately 10^{-2} M solution, they were diluted in water to prepare solutions with several different concentration. Either HDM2(11–119) or GST-HDMX(1–188) (2.2 μM) was incubated with 30 nM fluorescein-labeled human p53(15–29) in 10 mM Tris–HCl (pH 7.6), 150 mM NaCl, 0.50 mM EDTA, and 2 mM β-mercaptoethanol at room temperature 1 h or 4 °C overnight. Experiments were performed with a 70-fold molar excess of protein over labeled p53-peptide to ensure that the peptide is completely bound by the protein. Under these conditions, there is no difference in the minimum fluorescence polarization values between direct and competition assays.[37] Fluorescence anisotropy was measured at 25 °C on a Beacon 2000 (PanVera, Madison, WI). Data points were measured in triplicate. IC_{50} values were calculated by nonlinear regression curve fitting indicated by the following formula using KALEIDA GRAPH 4.0 software (Synergy Software, Reading, PA):

$$y = y_{\min} + \frac{(y_{\max} - y_{\min})}{1 + \left(\frac{x}{IC_{50}}\right)^{z}}$$

where $y_{\min}$, $y_{\max}$ are the observed fluorescence polarization values when the fluorescein-conjugated p53 peptide was completely bound or not bound to HDM2 and HDMX, respectively, and x and z are the competitor concentration and a slope factor, respectively. The IC_{50} values for p53(15–29) binding to HDM2 and HDMX were 1–2 μM. For Nutlin-3a the IC_{50} values were 1 μM and 6–7 μM for HDM2 and HDMX, respectively. Nutlin compounds were generous gifts from Dr. L. T. Vassilev and Hoffman-LaRoche, Inc., Nutley, NJ.

3. Results

3.1. NAPA synthesis

All NAPA molecules were synthesized by solid phase synthesis on TentaGel resin with a Rink amide linker. The first residue attached to the resin was Fmoc-β-alanine which served as a linker to facilitate the subsequent steps. After removal of the Fmoc group, a reductive amination between the primary amine on solid support and an Fmoc-protected α-amino aldehyde (Scheme 1)[38,39] was carried out using $NaBH(OAc)_3$ as a reducing reagent. Then, an isocyanate was reacted with the secondary amine on solid support, resulting in formation of the urea bond. The sequence of Fmoc deprotection, reductive amination, and urea formation was repeated until the desired oligomer length was achieved. Cleavage of the NAPA from the resin was accomplished with an aqueous solution of TFA and TIS as scavengers, and the product was precipitated by addition of diethyl ether. The crude material was purified by reverse phase HPLC using a C4 preparative column.

In the HPLC profiles of each NAPA, multiple peaks with slightly different retention times were observed and each peak had the molecular mass of the intended molecule. For several NAPAs, each peak with the correct molecular weight was purified and then reanalyzed by HPLC. In each case the purified material eluted at its original retention time, indicating that each peak represents a constitutional isomer of the same molecule. The most likely explanation for the observation of multiple peaks with the same mass is that racemization occurred at some point during synthesis. Racemization was further confirmed in NAPA 25 where the molecule was made from either L- or D-glutamic acid. Isolation of each peak in the HPLC followed by 1D ^{1}H NMR analysis showed that at least two HPLC peaks from each synthesis had identical NMR spectra. Several attempts were made to isolate each HPLC peak of NAPA 25 (Fig. 7) in sufficient quantity for more detailed analysis by NMR so that the structure and stereochemistry could be assigned. The spectra of each of the three peaks from NAPA 25 were complex and suffered from extensive spectral overlap, which prevents mak-

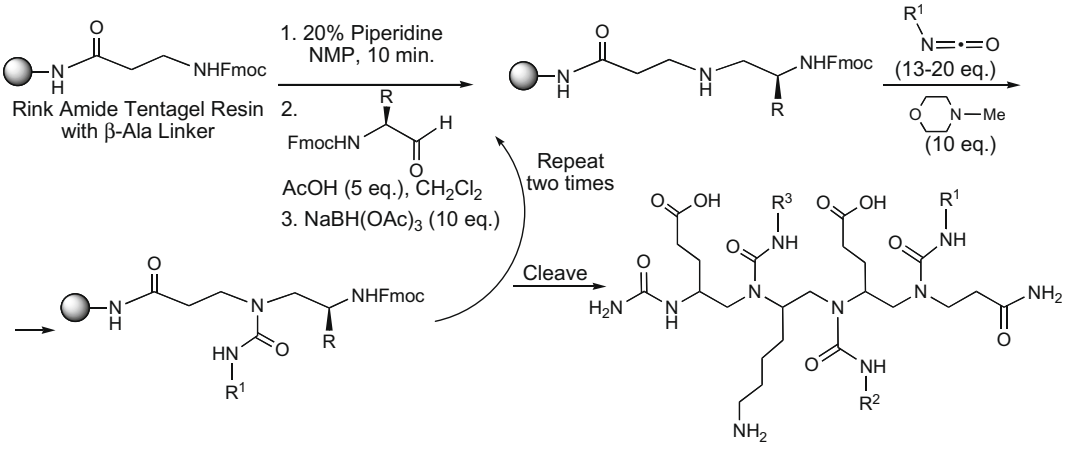

Scheme 1. General synthetic strategy for NAPA synthesis.

ing specific assignments to resonances (see Supplementary data). Comparison of the spectra indicate that each HPLC peak represents a molecule with a similar structure but also indicates that each peak could itself be a mixture of diastereomers. With three stereogenic centers in each NAPA, the theoretical number of possible diastereomers for each NAPA is 8. In the absence of more concrete evidence, it is prudent to assume that each synthesis yields a mixture of all possible diastereomers.

While racemization occurs during synthesis, this does not appear to be detrimental to inhibition of HDM2 or HDMX association with p53 (as presented below). Unless otherwise specified, each NAPA molecule was isolated as a mixture of several HPLC peaks with identical mass and this mixture of diastereomers was tested for inhibitory activity. The stereochemistry is purposely left undefined in the molecular structures shown below to highlight this aspect of the study. For the most active NAPAs, each peak was isolated by HPLC and tested individually for inhibition. As described below, the stereochemistry of the backbone did not significantly alter the inhibition properties of the molecule.

3.2. Initial NAPA design

The initial strategy to develop a NAPA into an inhibitor of HDM2–p53 binding centered on reproducing the relative positioning of the F19, W23 and L26 residues of the p53 peptide that binds to the protein. Therefore, hydrophobic sidechains were attached to the three urea groups projecting off the NAPA backbone to orient them into the hydrophobic binding cleft (as represented by Fig. 1). The sidechains directly attached to the carbons in the backbone were chosen to be hydrophilic to maintain aqueous solubility and to potentially form stabilizing salt bridges with the protein. Based on a cursory analysis of the surface of HDM2, it seemed that the incorporation of two glutamic acid sidechains and a lysine could result in favorable charge–charge interactions with surface residues of the protein. For the first round of NAPAs, inhibition of only p53–HDM2 was examined. Attempts to closely mimic the hydrophobic groups of p53 (which involved placing an indole sidechain on the central urea of the NAPA) did not result in any inhibition of HDM2–p53 association. The synthetic scheme to make this scaffold allowed numerous other groups to be attached and different linker lengths to be explored. As shown in Figure 2, increasing the distance between the hydrophobic sidechains and the ureas as well as incorporating different halogens on the aromatic rings helped to achieve the first weak inhibitor of p53–HDM2 binding (entry 5). This molecule, however, was not able to inhibit p53–HDMX binding.

3.3. Optimization to inhibit HDM2 and HDMX binding to p53

To achieve inhibition of HDMX binding to p53, a number of additional NAPA sidechains were examined in which different *para*-substituents at positions X and Y were introduced. Eventually it was concluded that the central sidechain should be fixed with a *para*-bromo phenyl ring (X = Br) as this group routinely afforded moderate inhibition of HDM2–p53 binding. The next series of studies focused on variations at position Y as well as small changes in linker length (Fig. 3), and ultimately it was found that a halogen at position Y is crucial for inhibition of HDMX–p53. In particular, NAPA 9, which has a bromine at position Y, inhibited HDM2 and HDMX binding with p53 two to four times better than a derivative with a hydrogen at the same position (NAPA 5). Replacing the bromine with a methyl group at the same position (entry 10) did not significantly affect the inhibitory activity towards HDMX, but activity against HDM2 decreased by three times. Since the effective van der Waals radii of methyl and bromo groups are very similar (1.80 and 1.86 Å, respectively) but their hydrogen bonding propensities are different,[40] it is possible that the substituent at this position engages in different interactions when binding to HDM2 versus HDMX. When the bromine at position Y was combined with a slightly longer linker (at position m), modest inhibition of both protein–protein interactions was achieved (entry 13). For this and all subsequent studies, inhibition of HDMX–p53 binding and HDM2–p53 binding was determined for each molecule and IC_{50} values for both protein–protein interactions are shown.

In the next series of NAPAs, the alkyl hydrophobic sidechain was replaced with an aromatic group so that different substituents could be examined at position Z (Fig. 4). Once again, the *p*-bromo phenyl group was optimal (entry 17), as other substituents lead to reduced inhibitory activity towards HDMX. Ultimately it was determined that a hydrophobic sidechain terminating with a cyclohexyl group was better than an aromatic ring with a substituent at position Z (entry 18, Fig. 5). These results suggest that the cyclohexyl group may form a hydrophobic interaction on the protein surface.

With an optimized set of hydrophobic sidechains, the effects of different modifications at the N-terminus of the NAPAs were explored. As shown in Figure 5, some hydrophobic sidechains at this position moderately improved inhibitory activity, while others decreased activity. From these results, the NAPA bearing an isopentanoyl group (entry 23) had the optimum activity, and this group was maintained in all subsequent derivatives.

At this point, reoptimization of the sidechains with the aromatic rings was briefly examined with the goal of reducing the number of

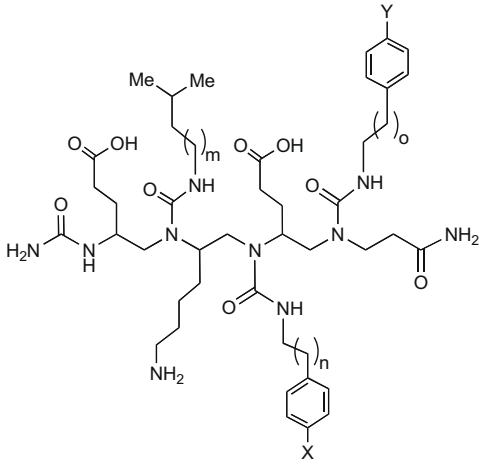

Entry	m	n	o	X	Y	IC_{50} (HDM2)[a]
1.	1	1	1	Cl	H	> 100
2.	2	1	1	Cl	H	85 ± 10
3.	2	1	1	Cl	Cl	63 ± 13
4.	2	1	2	Cl	H	43 ± 8
5.	2	1	2	Br	H	18 ± 2[b]
6.	2	2	2	Br	H	20 ± 3
7.	2	2	1	H	Br	38 ± 6

[a] All values reported in μM.
[b] IC_{50} (HDMX) = 96 ± 4 μM

Figure 2. Initial development of NAPAs to inhibit HDM2. The initial NAPA scaffold was modified with halogens and varying lengths of sidechain linkers.

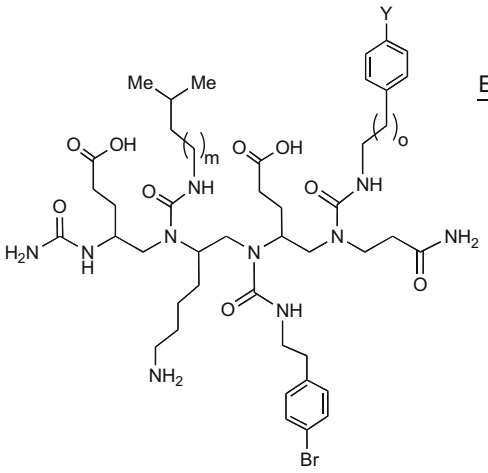

Entry	m	o	Y	IC_{50} (HDM2)[a]	IC_{50} (HDMX)[a]
8.	2	1	Br	17 ± 2	41 ± 3
9.	2	2	Br	9.2 ± 0.4	24 ± 2
10.	2	2	Me	24 ± 3	36 ± 3
11.	2	2	NO_2	41 ± 10	59 ± 4
12.	2	2	OMe	>100	>100
13.	3	2	Br	13 ± 1	13 ± 1

[a] All values reported in μM.

Figure 3. Extension of NAPAs to inhibit HDMX by introduction of substituents at Y and variation in sidechain lengths.

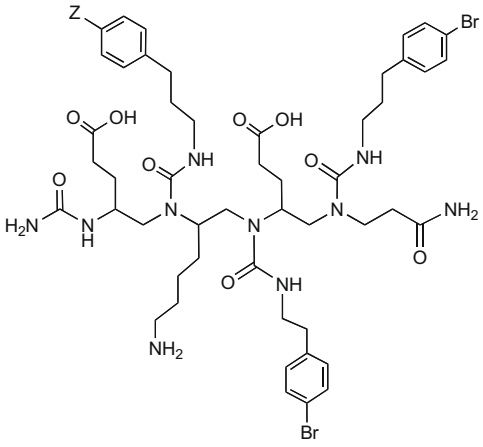

Entry	Z	IC_{50} (HDM2)[a]	IC_{50} (HDMX)[a]
14.	H	13 ± 1	20 ± 1
15.	OMe	12 ± 1	12 ± 1
16.	NO_2	10 ± 1	8.1 ± 0.4
17.	Br	8.2 ± 0.3	7.5 ± 0.9

[a] All values reported in μM.

Figure 4. Examination of the effects on inhibition of substituents at position Z.

bromine atoms at positions X and Y (Fig. 6). While the bromine at position X could be replaced with a methyl group without compromising activity for inhibition of HDM2–p53, activity against HDMX–p53 decreased slightly. Therefore, the bromine at position X was retained. In contrast, replacement of the bromine atom at position Y with fluorine resulted in a slight improvement of the activity for inhibition of HDMX–p53. From this study, the best NAPA for inhibition of HDM2 and HDMX binding to p53 is the one represented by entry 25.

3.4. Contributions to activity from stereochemistry, amino acid sidechains, and ureas

With the NAPA from entry 25 (NAPA 25, Fig. 6) identified as an optimized inhibitor of HDM2 and HDMX association with p53, efforts were directed toward determining the specific features of this molecule responsible for the activity. As mentioned previously, each NAPA oligomer displayed multiple peaks on HPLC purification that are diastereomers which likely form as a result of racemiza-

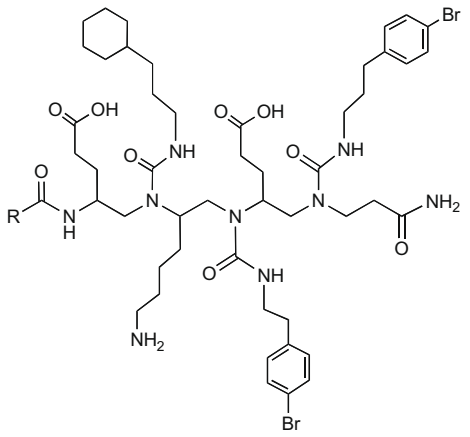

Entry	R	IC_{50} (HDM2)[a]	IC_{50} (HDMX)[a]
18.	NH_2	6.4 ± 1.2	6.5 ± 1.3
19.	PhNH	10.5 ± 0.3	7.6 ± 0.4
20.	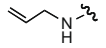	17 ± 2	10 ± 1
21.	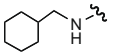	6.6 ± 1.2	8.0 ± 0.5
22.		8.2 ± 0.3	10 ± 1
23.	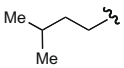	2.8 ± 0.1	4.1 ± 0.5
24.	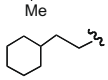	2.8 ± 0.2	7.5 ± 1.8

[a] All values reported in μM.

Figure 5. Optimization of N-terminal group for inhibition of p53 binding to HDM2 and HDMX.

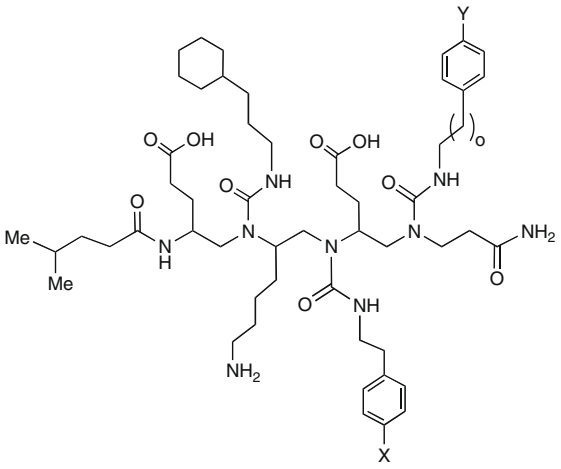

Entry	o	X	Y	IC_{50} (HDM2)[a]	IC_{50} (HDMX)[a]
25.	2	Br	F	2.6 ± 0.2	2.7 ± 0.1
26.	2	Me	Br	2.3 ± 0.1	3.2 ± 0.1
27.	2	Me	F	2.9 ± 0.6	5.1 ± 0.6
28.	3	Me	F	13 ± 1	14 ± 1

[a] All values reported in μM.

Figure 6. Re-optimization of the sidechains at positions X and Y.

tion. For all the previous inhibition results, multiple HPLC peaks of each NAPA were collected and tests for inhibition were performed using a diastereomeric mixture. For NAPA 25, each HPLC peak was separated and independently tested for inhibition of both HDM2 and HDMX binding to p53. In addition, the same NAPA was made using D-glutamic acid instead of the L-form and HPLC peaks were separated and independently tested. As shown in Figure 7A, NAPA 25 made from L-Glu showed three peaks by HPLC and the inhibitory activity was similar for each peak (entries 29–31). NAPA 25 made from D-Glu showed predominantly two HPLC peaks and each one inhibited similarly (entries 32 and 33). These results indicate that the stereochemistry of the NAPA backbone does not significantly affect inhibitory activity.

The next goal centered on exploring the importance of the hydrophilic amino acid sidechains to inhibition. Originally, these sidechains were present to simply promote aqueous solubility. In the first experiment, the glutamic acid sidechains were changed to L-homo-glutamic acid sidechains (NAPA 34, Fig. 8). HPLC analysis showed this molecule as a single peak, suggesting that racemization occured at the stereocenters bearing the glutamic acid sidechains in the previous NAPAs. Unfortunately, the homo-glutamic acid sidechains had a negative impact on inhibitory activity, especially for HDMX–p53 association. Replacing all the amino acid sidechains with lysines (NAPA 35) eliminated all inhibitory activity. Therefore, the arrangement of amino acid sidechains is important for the activity of NAPA 25.

In the final series of studies, the importance of the ureas was investigated by systematically replacing each one with a tertiary amine (Fig. 9). Eliminating all ureas resulted in a molecule with no inhibitory activity (entry 36). Replacing one urea with a tertiary amine resulted in decreased inhibitory activity as well, but replacement of the central urea caused the most significant decrease. For these studies (entries 37–39), each peak was isolated by HPLC and each one was tested for activity. In most cases, the activity of each

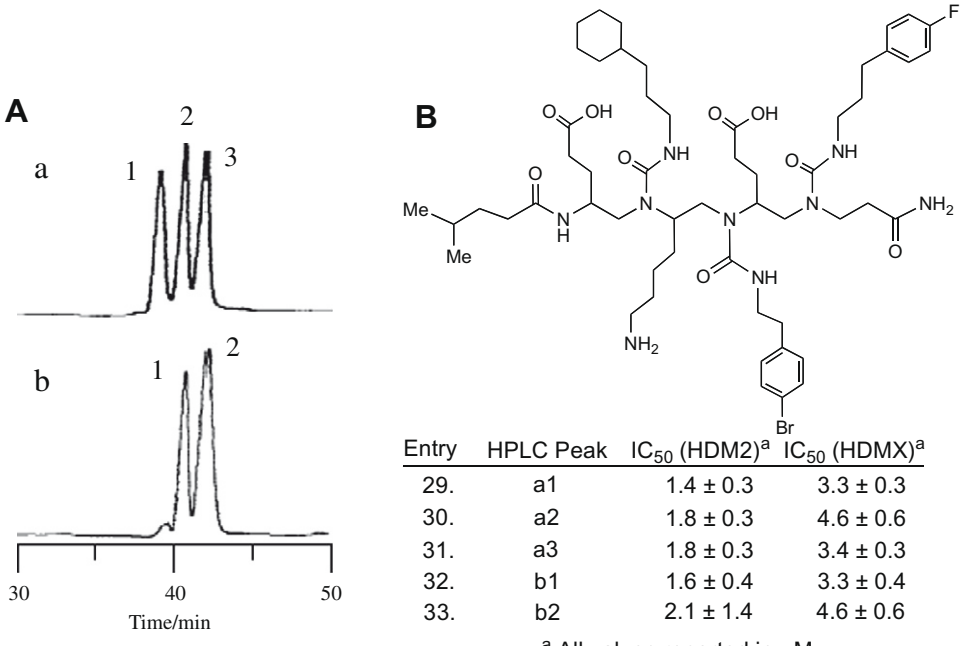

Entry	HPLC Peak	IC_{50} (HDM2)[a]	IC_{50} (HDMX)[a]
29.	a1	1.4 ± 0.3	3.3 ± 0.3
30.	a2	1.8 ± 0.3	4.6 ± 0.6
31.	a3	1.8 ± 0.3	3.4 ± 0.3
32.	b1	1.6 ± 0.4	3.3 ± 0.4
33.	b2	2.1 ± 1.4	4.6 ± 0.6

[a] All values reported in μM.

Figure 7. Separation and inhibitory activity of NAPA 25. (A) HPLC profiles of NAPA 25 synthesized from all L-amino acids (a) or D-glutamic acid and L-lysine (b). HPLC separation was performed as described in Experimental section. (B) Structure of NAPA 25 and inhibition data for separated peaks.

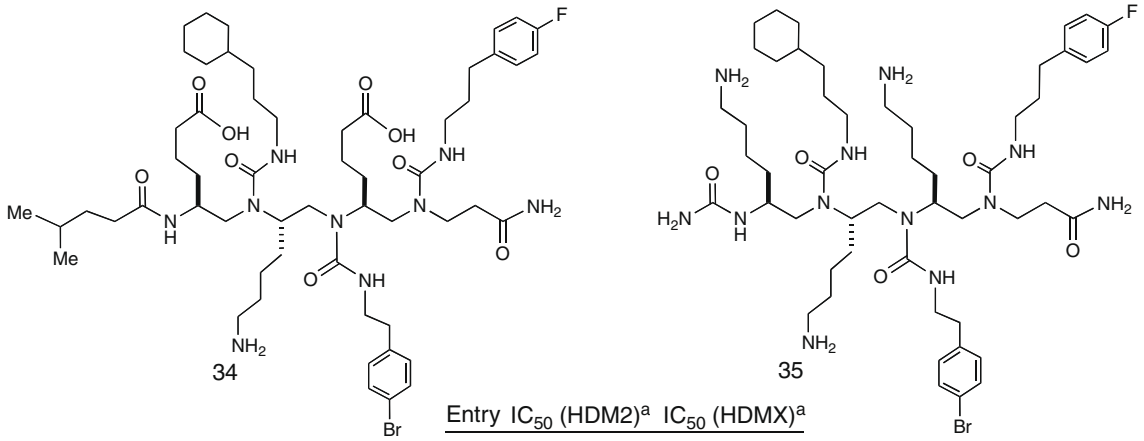

Entry	IC_{50} (HDM2)[a]	IC_{50} (HDMX)[a]
34.	5.9 ± 0.4	41 ± 1
35.	No Inhibition	No Inhibition

[a] All values reported in μM.

Figure 8. Analog of NAPA 25 with L-homo-glutamic acid and L-lysine.

peak was similar (as previously described for NAPA 25) although two peaks of entry 38 completely lost the ability to inhibit HDM2–p53.

3.5. Molecular modeling of the HDM2 and HDMX complex of NAPA25

To model the complex of NAPA25 with HDM2 and HDMX, a few general assumptions were made based on the results above and literature precedent. First, complexes were modeled such that the hydrophobic sidechains of the NAPAs bind in the clefts of the proteins in a manner similar to the p53 peptide. There is ample precedent in the literature demonstrating that burial of hydrophobic surface area drives binding of ligands to HDM2, and it is likely that similar forces direct binding to HDMX.[10,11,20,22,31,41] In addition, results with a number of different NAPAs illustrate that the relative lengths of hydrophobic sidechains influences binding affinity (compare NAPAs 8, 9, and 13 in Fig. 3; and 27 and 28 in Fig. 6). To highlight the importance of sidechain length, Figure 10 provides a comparison of the hydrophobic groups that project off from the p53 peptide and NAPA 25 as modeled in an extended conformation. In this figure, the two horizontal lines represent the bottom of the hydrophobic cleft of HDM2. In panel A, the relative depths of the F19, W23 and L26 residues of p53 are presented, with the tryptophan sidechain reaching the bottom of the hydrophobic cleft of HDM2. As seen in panel B, these relative distances are approximately maintained in the extended structure of NAPA 25. From this perspective, the NAPA molecule's hydrophobic sidechains fill the hydrophobic clefts of HDM2 (and HDMX) with the bromine atom of the central sidechain reaching the bottom of the cleft. Therefore, all models were constructed with the sidechain of the central urea group (including the bromine atom) bound in the central pocket of the hydrophobic cleft. With this sidechain anchored into the binding pocket, two main conformations of the complex were examined: one with the long axis of the inhibitor running the length of the cleft and the other with the molecule rotated 180° around the static central sidechain.

Another assumption for modeling the complexes was that the three urea groups of the NAPA form two, tandem hydrogen bonds, as shown in Figures 1 and 10B. Based on the previous work by Nowick and co-workers,[25] this backbone conformation is accessible. The importance of the ureas is also supported by the results demonstrating that inhibition is severely weakened when the urea groups are removed (Fig. 9). We believe that the hydrogen bonds help to align all three non-polar residues along the same side of the inhibitor and therefore maximize solvent exclusion from the cleft, enhancing binding affinity. In this conformation, the NAPAs adopt a β-sheet-like conformation that is similar to structures determined for *N,N″*-trisubstituted diethylenetriamines.[25]

Even with the two previous assumptions in place, there are still many plausible ways to dock NAPA 25 to HDM2 and HDMX due to the flexibility of the sidechains. The four structures in Figure 11 represent the most likely scenarios for binding based on modeling NAPA 25 with all L-stereochemistry in the backbone (L-NAPA 25). While other diastereomers were not extensively examined, a cursory examination indicated that backbone stereochemistry has little impact on the orientations of the groups at the ends of the urea sidechains. In this figure, panels A and B represent binding of L-NAPA 25 to HDM2 in two different orientations that differ by 180° about the central sidechain while panels C and D represent the same molecule bound in both ways to HDMX. In all cases, the deepest point of the cleft is filled with the *p*-bromophenyl sidechain, which is important for binding to both proteins (Figs. 2 and 6). Although this differs from an indole group, which would be most similar to W23 of p53, it resembles the crystal structure of Nutlin 2 bound to HDM2.[14] Other studies have also shown that a halogen at the 6 position of W23 in the p53 peptide nicely fills this pocket and enhances the binding affinity.[41] As the cyclohexane and *p*-fluorophenyl sidechains of NAPA 25 (Fig. 6) differ from the F19 and L26 residues of p53,[31,32] alternative binding modes that are not analogous to other known HDM2 ligands likely dictate the binding of NAPA 25. In panels A and C of Figure 11, the cyclohexane sidechain is buried in the location occupied by F19 of p53, and the *p*-fluorophenyl is in the location of L26. Such a model could explain the preference for a bromine or fluorine substituent on the phenyl group of this sidechain (in accordance with the data in Fig. 3 for different substituents at position Y). A halogen at this position could engage in a favorable electrostatic interaction with the hydroxyl group of the proximal tyrosine residue, Y100 of HDM2 or Y99 of HDMX, or alternatively, penetrate deeper into smaller sub-cavities at this location. At the N-terminus of the molecule, the hydrophobic sidechain covers extra non-polar surface area at the periphery of the cleft, which could explain the preference for a non-polar residue at this location (see Fig. 5). This model also demonstrates that the negatively-charged glutamic acid residues of L-NAPA 25 form salt bridges with H73 and K94 of HDM2 and K50 of HDMX, which

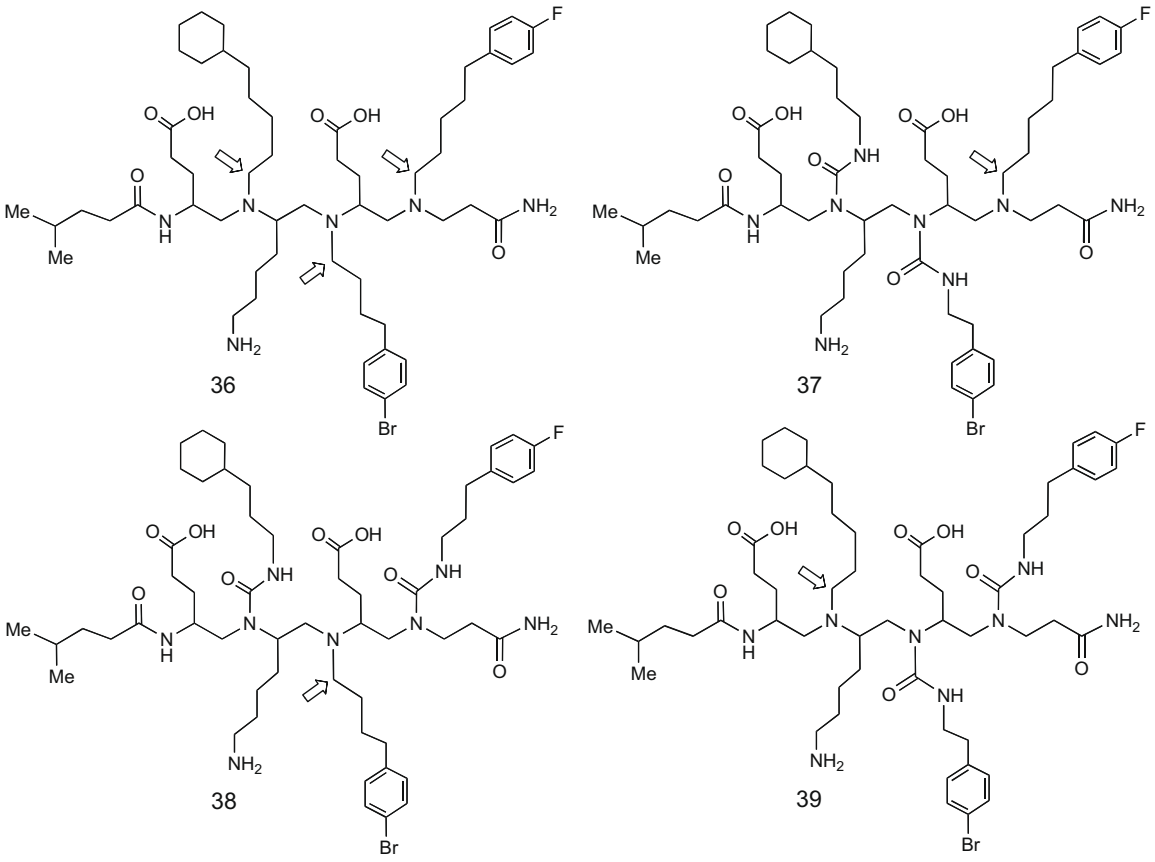

Entry	Number of Ureas	Number of HPLC Peaks	IC_{50} (HDM2)[a]	IC_{50} (HDMX)[a]
36.	0	1	>100	>100
37.	2	2	12 ± 3	31 ± 3
			8 ± 3	34 ± 4
38.	2	4	>100	36 ± 6
			38 ± 3	22 ± 4
			23 ± 4	26 ± 4
			>100	15 ± 4
39.	2	3	7.3 ± 0.7	24 ± 1
			6.1 ± 0.4	19 ± 3
			4.7 ± 0.3	14 ± 3

[a] Inhibitory values for each HPLC peak are reported in μM.

Figure 9. Effect of replacing urea groups on inhibition of HDM2 and HDMX binding to p53. The arrows designate the location where a urea has been replaced with an amine. In cases where multiple HPLC peaks were present, each peak was separated and the inhibition tested for each individual peak.

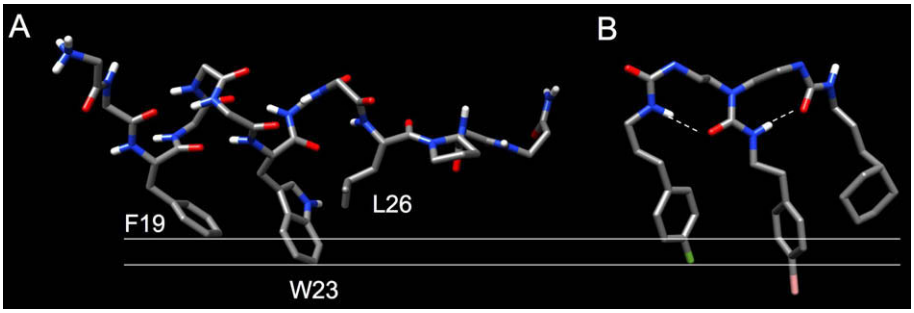

Figure 10. Comparison of the sidechain lengths of (A) HDM2-bound p53 (1YCR.pdb) and (B) extended NAPA 25. The horizontal white lines denote the extents of the F19 and W23 residues of p53. Only the cleft-binding sidechains of each molecule are shown for clarity. The proposed, intramolecular hydrogen bonds among the three, main urea groups of NAPA 25 are illustrated by dashed white lines.

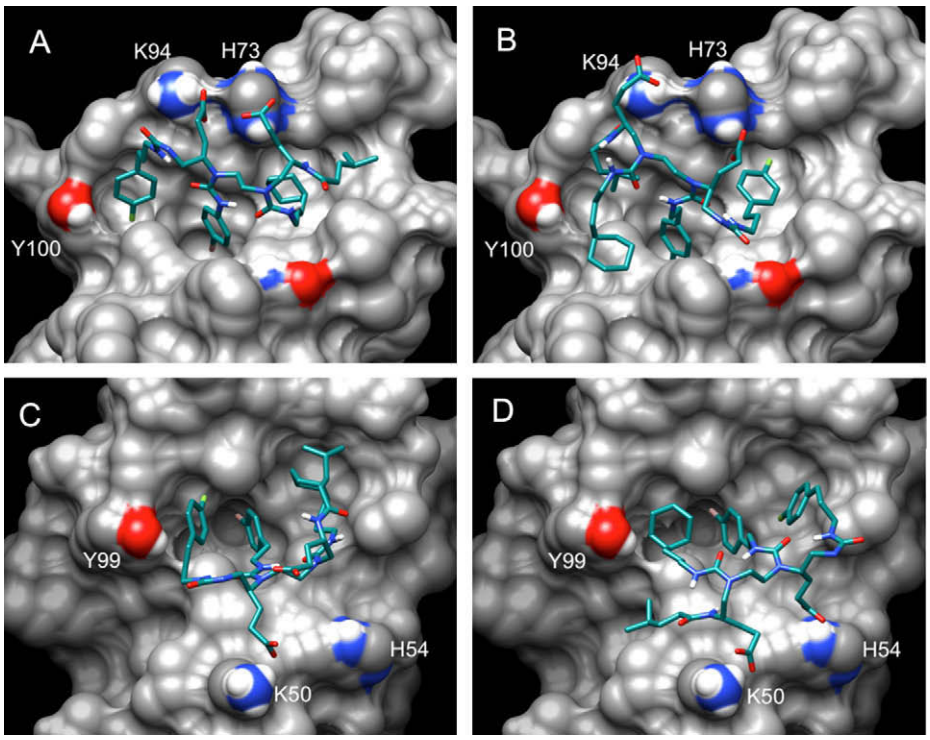

Figure 11. Models for binding of L-NAPA 25 to HDM2 (1RV1.pdb, chain A) (panels A and B) and HDMX (3EQY.pdb, chain A) (panels C and D). For clarity, the lysine and glutamine-like sidechains of the NAPA molecule, which are simply exposed to solvent, have been omitted from the illustrations.

could explain why these sidechains are important for inhibition (consistent with data in Fig. 8).

In the alternative models shown in panels B and D (where the inhibitor is rotated 180° about the central sidechains), similar salt bridges are present between the charged sidechains of L-NAPA 25 and several residues of HDM2 and HDMX. In the complex with HDM2 shown in panel B, the hydrophobic (leucine-like) sidechain at the N-terminus of the inhibitor occupies the same location as L26 of the bound p53 peptide. In this case, the cyclohexane group covers an additional region of proximally exposed non-polar surface area of the cleft. In the complex with HDMX shown in panel D, the preferred model has the positions of the cyclohexane and N-terminal hydrophobic groups switched so that the cyclohexane occupies the site typically bound by L26 of p53.

4. Discussion

We have developed a NAPA scaffold that can be used to target families of closely related protein–protein interactions. The interfaces at which proteins recognize one another often consist of a combination of hydrophobic patches and electrostatic complementarity.[42] Developing inhibitors that mimic such interfaces is notoriously challenging. Among the molecules developed to target HDM2, most approaches use a rigid molecular scaffold to maximize the hydrophobic contacts with the protein to attain high affinity and specificity.[12,13,17] While these strategies have resulted in excellent inhibitors of HDM2–p53, the success has been at the expense of HDMX–p53 inhibition. In the case of Nutlin-3, the difference in the locations of a single tyrosine between proteins is enough to allow excellent binding to HDM2 and at the same time significantly curtail binding to HDMX.[21] Due to its rigid scaffold, Nutlin is not able to adapt to the altered binding pocket of HDMX. Oligomeric molecules, such as the β-peptides developed by Schepartz and co-workers,[24,43,44] offer the possibility of simultaneously targeting related families of protein–protein interactions because the flexibility of the scaffolds can allow the conformation of the molecules to adapt to slightly different binding pockets. Despite these advances, most oligomeric inhibitors of protein–protein interactions are large molecules that would be extremely difficult to produce in sufficient quantities for drug development. In contrast, NAPAs offer the possibility of using a short oligomeric scaffold that is densely functionalized with both hydrophobic and hydrophilic groups. After several rounds of optimization, a single trimeric inhibitor was developed that equally inhibits HDM2 and HDMX binding to p53 with IC_{50} values in the low micromolar range. Since the current synthesis yields a diastereomeric mixture of molecules, clearly an alternative route to these molecules is needed and new strategies are being examined in this regard. At the same time, different diastereomers do not have markedly different inhibition properties. This is likely due to the highly flexible sidechains which can orient the terminal groups in similar conformations regardless of the chirality present in the backbone.

Molecular modeling suggests that the ability of L-NAPA 25 to alter its conformation between the binding pockets of HDM2 and HDMX allows for equivalent inhibition of the two proteins. The models also highlight the ability of this inhibitor to simultaneously engage in hydrophobic interactions with the protein binding pockets and electrostatic interactions with polar residues that line the peripheries of the binding clefts. Maximizing both sets of interactions on a scaffold that retains some flexible characteristics may be an important criterion in future strategies to find inhibitors of protein–protein interactions.

Acknowledgements

This research was supported in part by the following Intramural Research Programs of the NIH: NCI Center for Cancer Research, NIDDK Laboratory of Bioorganic Chemistry. We gratefully acknowledge Dr. Lisa Jenkins and George Leiman for assistance with the preparation of this manuscript.

Supplementary data

Supplementary data (synthetic procedures and characterization for all NAPAs) associated with this article can be found, in the online version, at doi:10.1016/j.bmc.2009.10.032.

References and notes

1. Chene, P. *Curr. Med. Chem. Anticancer Agents* **2001**, *1*, 151.
2. Momand, J.; Wu, H. H.; Dasgupta, G. *Gene* **2000**, *242*, 15.
3. Vogelstein, B.; Lane, D.; Levine, A. J. *Nature* **2000**, *408*, 307.
4. Han, X.; Garcia-Manero, G.; McDonnell, T. J.; Lozano, G.; Medeiros, L. J.; Xiao, L.; Rosner, G.; Nguyen, M.; Fernandez, M.; Valentin-Vega, Y. A.; Barboza, J.; Jones, D. M.; Rassidakis, G. Z.; Kantarjian, H. M.; Bueso-Ramos, C. E. *Mod. Pathol.* **2007**, *20*, 54.
5. Ramos, Y. F.; Stad, R.; Attema, J.; Peltenburg, L. T.; van der Eb, A. J.; Jochemsen, A. G. *Cancer Res.* **2001**, *61*, 1839.
6. Wade, M.; Wong, E. T.; Tang, M.; Stommel, J. M.; Wahl, G. M. *J. Biol. Chem.* **2006**, *281*, 33036.
7. Stad, R.; Ramos, Y. F.; Little, N.; Grivell, S.; Attema, J.; van Der Eb, A. J.; Jochemsen, A. G. *J. Biol. Chem.* **2000**, *275*, 28039.
8. Marine, J. C.; Dyer, M. A.; Jochemsen, A. G. *J. Cell Sci.* **2007**, *120*, 371.
9. Hu, B.; Gilkes, D. M.; Chen, J. *Cancer Res.* **2007**, *67*, 8810.
10. Kussie, P. H.; Gorina, S.; Marechal, V.; Elenbaas, B.; Moreau, J.; Levine, A. J.; Pavletich, N. P. *Science* **1996**, *274*, 948.
11. Bottger, A.; Bottger, V.; Garcia-Echeverria, C.; Chene, P.; Hochkeppel, H. K.; Sampson, W.; Ang, K.; Howard, S. F.; Picksley, S. M.; Lane, D. P. *J. Mol. Biol.* **1997**, *269*, 744.
12. Hu, C. Q.; Hu, Y. Z. *Curr. Med. Chem.* **2008**, *15*, 1720.
13. Murray, J. K.; Gellman, S. H. *Biopolymers* **2007**, *88*, 657.
14. Vassilev, L. T.; Vu, B. T.; Graves, B.; Carvajal, D.; Podlaski, F.; Filipovic, Z.; Kong, N.; Kammlott, U.; Lukacs, C.; Klein, C.; Fotouhi, N.; Liu, E. A. *Science* **2004**, *303*, 844.
15. Wade, M.; Rodewald, L. W.; Espinosa, J. M.; Wahl, G. M. *Cell Cycle* **2008**, *7*, 1973.
16. Shangary, S.; Qin, D.; McEachern, D.; Liu, M.; Miller, R. S.; Qiu, S.; Nikolovska-Coleska, Z.; Ding, K.; Wang, G.; Chen, J.; Bernard, D.; Zhang, J.; Lu, Y.; Gu, Q.; Shah, R. B.; Pienta, K. J.; Ling, X.; Kang, S.; Guo, M.; Sun, Y.; Yang, D.; Wang, S. *Proc. Natl. Acad. Sci. U.S.A.* **2008**, *105*, 3933.
17. Saraogi, I.; Hamilton, A. D. *Biochem. Soc. Trans.* **2008**, *36*, 1414.
18. Kitagaki, J.; Agama, K. K.; Pommier, Y.; Yang, Y.; Weissman, A. M. *Mol. Cancer. Ther.* **2008**, *7*, 2445.
19. Wang, Y. V.; Wade, M.; Wong, E.; Li, Y. C.; Rodewald, L. W.; Wahl, G. M. *Proc. Natl. Acad. Sci. U.S.A.* **2007**, *104*, 12365.
20. Popowicz, G. M.; Czarna, A.; Holak, T. A. *Cell Cycle* **2008**, *7*, 2441.
21. Popowicz, G. M.; Czarna, A.; Rothweiler, U.; Szwagierczak, A.; Krajewski, M.; Weber, L.; Holak, T. A. *Cell Cycle* **2007**, *6*, 2386.
22. Kallen, J.; Goepfert, A.; Blechschmidt, A.; Izaac, A.; Geiser, M.; Tavares, G.; Ramage, P.; Furet, P.; Masuya, K.; Lisztwan, J. *J. Biol. Chem.* **2009**, *284*, 8812.
23. Macchiarulo, A.; Pellicciari, R. *Expert Opin. Ther. Patents* **2009**, *19*, 721.
24. Harker, E. A.; Daniels, D. S.; Guarracino, D. A.; Schepartz, A. *Bioorg. Med. Chem.* **2009**, *17*, 2038.
25. Nowick, J. S.; Mahrus, S.; Smith, E. M.; Ziller, J. W. *J. Am. Chem. Soc.* **1996**, *118*, 1066.
26. Robinson, J. A. *Acc. Chem. Res.* **2008**, *41*, 1278.
27. Grasslin, A.; Amoreira, C.; Baldridge, K. K.; Robinson, J. A. *ChemBioChem* **2009**, *10*, 1360.
28. Fasan, R.; Dias, R. L.; Moehle, K.; Zerbe, O.; Obrecht, D.; Mittl, P. R.; Grutter, M. G.; Robinson, J. A. *ChemBioChem* **2006**, *7*, 515.
29. Fasan, R.; Dias, R. L.; Moehle, K.; Zerbe, O.; Vrijbloed, J. W.; Obrecht, D.; Robinson, J. A. *Angew. Chem., Int. Ed.* **2004**, *43*, 2109.
30. Berman, H. M.; Westbrook, J.; Feng, Z.; Gilliland, G.; Bhat, T. N.; Weissig, H.; Shindyalov, I. N.; Bourne, P. E. *Nucleic Acids Res.* **2000**, *28*, 235.
31. Pazgier, M.; Liu, M.; Zou, G.; Yuan, W.; Li, C.; Li, J.; Monbo, J.; Zella, D.; Tarasov, S. G.; Lu, W. *Proc. Natl. Acad. Sci. U.S.A.* **2009**, *106*, 4665.
32. Czarna, A.; Popowicz, G. M.; Pecak, A.; Wolf, S.; Dubin, G.; Holak, T. A. *Cell Cycle* **2009**, *8*, 1176.
33. Brooks, B. R.; Brooks, C. L., III; Mackerell, A. D., Jr.; Nilsson, L.; Petrella, R. J.; Roux, B.; Won, Y.; Archontis, G.; Bartels, C.; Boresch, S.; Caflisch, A.; Caves, L.; Cui, Q.; Dinner, A. R.; Feig, M.; Fischer, S.; Gao, J.; Hodoscek, M.; Im, W.; Kuczera, K.; Lazaridis, T.; Ma, J.; Ovchinnikov, V.; Paci, E.; Pastor, R. W.; Post, C. B.; Pu, J. Z.; Schaefer, M.; Tidor, B.; Venable, R. M.; Woodcock, H. L.; Wu, X.; Yang, W.; York, D. M.; Karplus, M. *J. Comput. Chem.* **2009**, *30*, 1545.
34. Morris, G. M.; Huey, R.; Lindstrom, W.; Sanner, M. F.; Belew, R. K.; Goodsell, D. S.; Olson, A. J. *J. Comput. Chem.* **2009**, *30*, 2785.
35. Pettersen, E. F.; Goddard, T. D.; Huang, C. C.; Couch, G. S.; Greenblatt, D. M.; Meng, E. C.; Ferrin, T. E. *J. Comput. Chem.* **2004**, *25*, 1605.
36. Hara, T.; Durell, S. R.; Myers, M. C.; Appella, D. H. *J. Am. Chem. Soc.* **2006**, *128*, 1995.
37. Plante, J. P.; Burnley, T.; Malkova, B.; Webb, M. E.; Warriner, S. L.; Edwards, T. A.; Wilson, A. J. *Chem. Commun.* **2009**, 5091.
38. Ho, P. T.; Ngu, K.-y. *J. Org. Chem.* **1993**, *58*, 2313.
39. Fukuyama, T.; Lin, S.-C.; Li, L. *J. Am. Chem. Soc.* **1990**, *112*, 7050.
40. Patani, G. A.; LaVoie, E. J. *Chem. Rev.* **1996**, *96*, 3147.
41. Garcia-Echeverria, C.; Chene, P.; Blommers, M. J.; Furet, P. *J. Med. Chem.* **2000**, *43*, 3205.
42. Wells, J. A.; McClendon, C. L. *Nature* **2007**, *450*, 1001.
43. Michel, J.; Harker, E. A.; Tirado-Rives, J.; Jorgensen, W. L.; Schepartz, A. *J. Am. Chem. Soc.* **2009**, *131*, 6356.
44. Harker, E. A.; Schepartz, A. *ChemBioChem* **2009**, *10*, 990.